# Biofunctional micellar nanoparticles from peptide-*b*-polymer chimeras

Charlotte Drappier,[a,b] Anne-Laure Wirotius,[a] Katell Bathany,[c] Emmanuel Ibarboure,[a] Olivia Condassamy,[a] Elisabeth Garanger*[a,b] and Sébastien Lecommandoux*[a]

**Figure S1: $^1$H NMR spectrum of $PTMC_{22}$ in $CD_2Cl_2$**

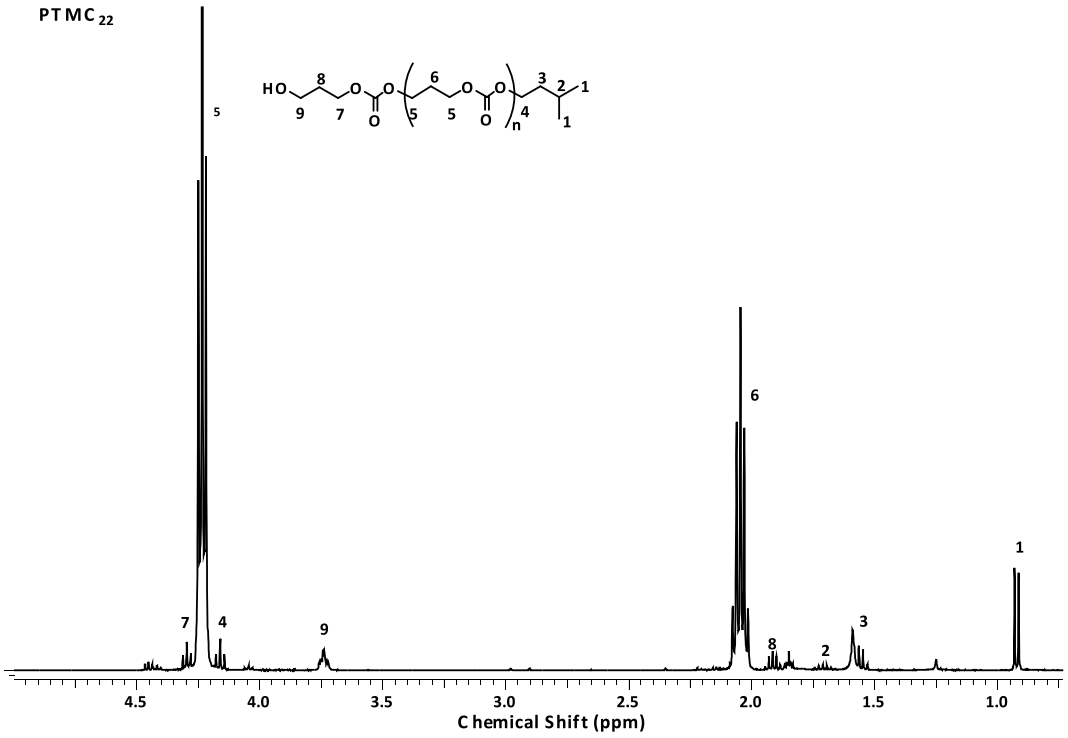


**Figure S2: $^1$H NMR spectrum of Mal-$PTMC_{22}$ in $CD_2Cl_2$**

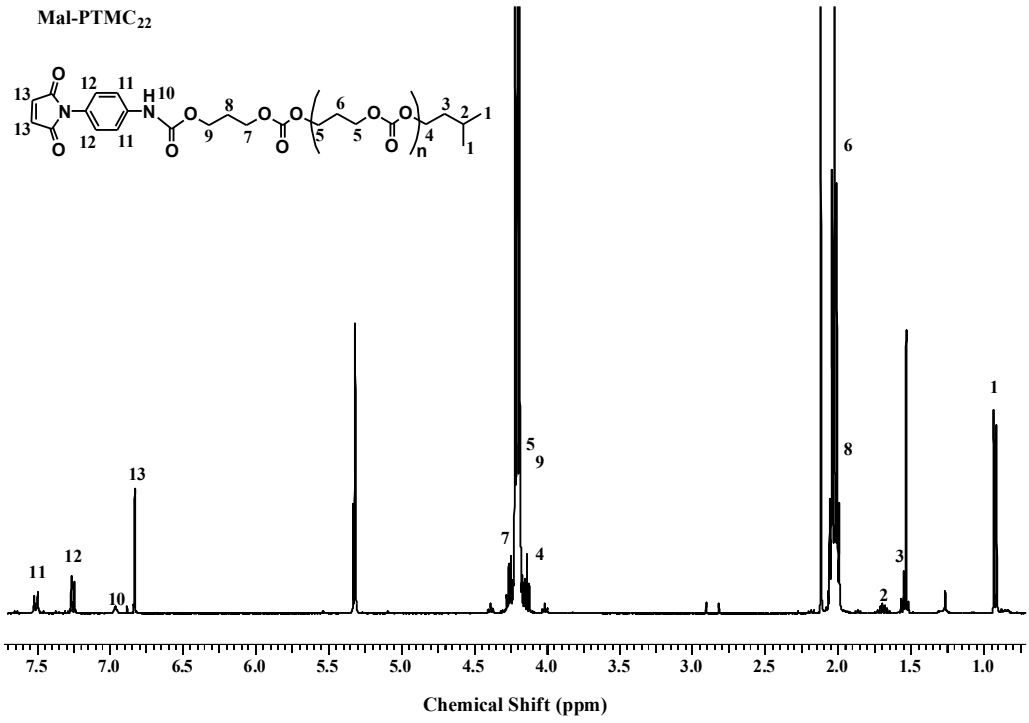

**Figure S3: HSQC NMR spectrum of Mal-PTMC$_{22}$ in DMSO**

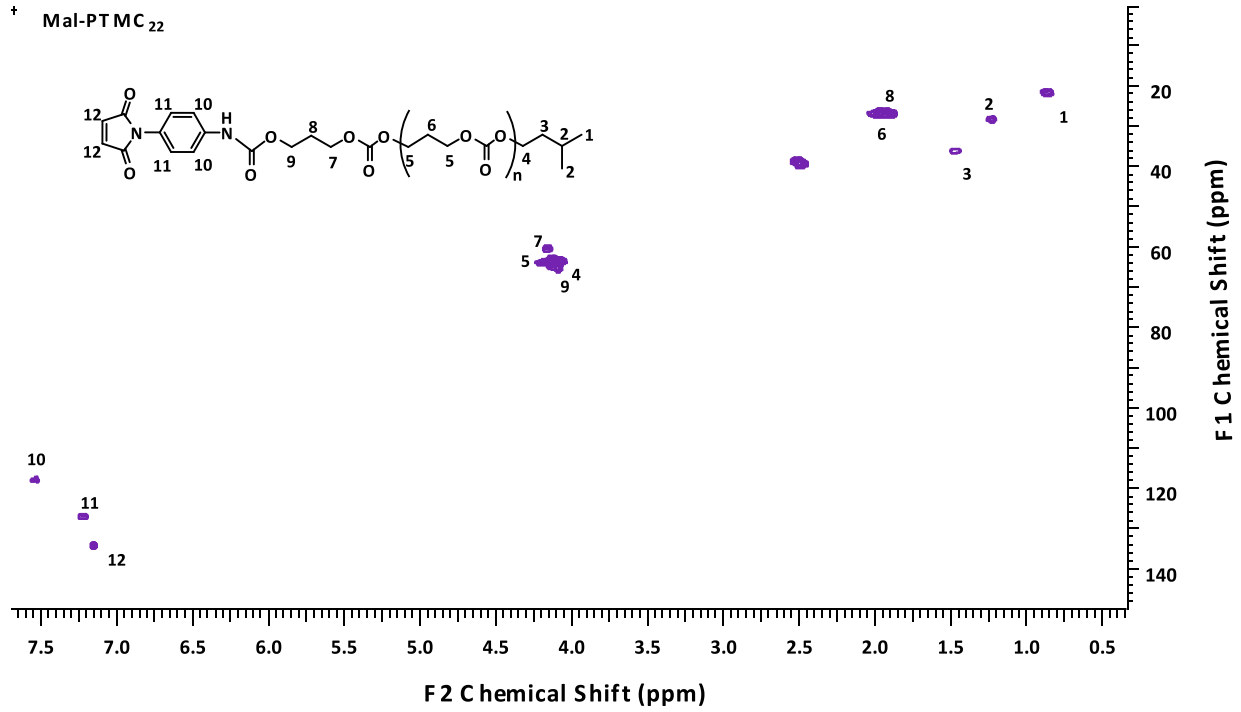


**Figure S4: $^{1}$H NMR spectrum of Tat-*b*-PTMC$_{22}$ in DMSO**

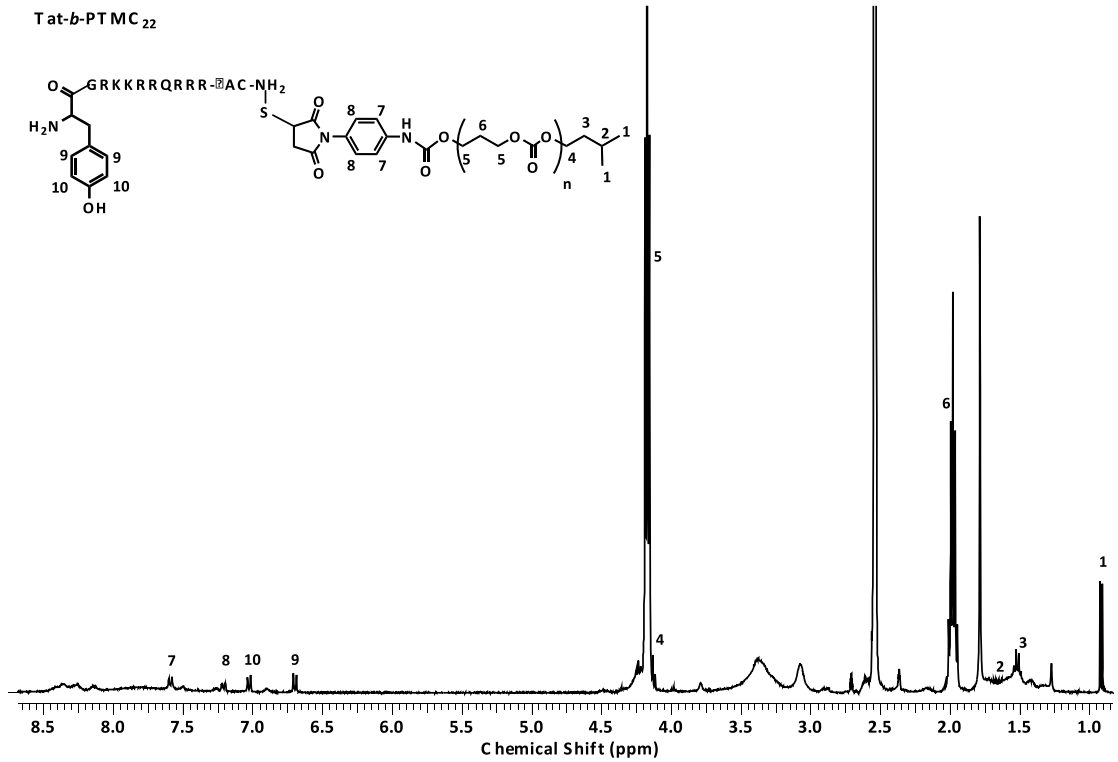

**Figure S5: HSQC NMR spectrum of Tat-*b*-PTMC$_{22}$ in DMSO**

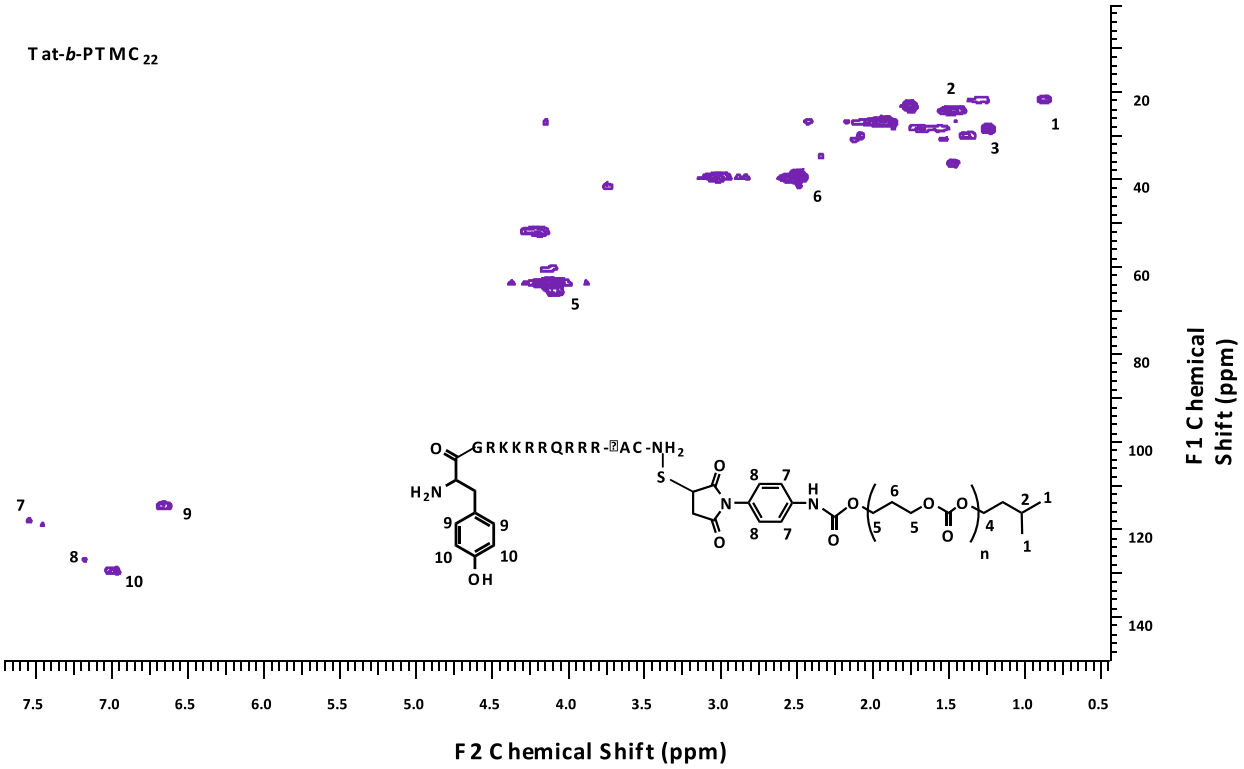


**Figure S6: MALDI-TOF spectrum of PTMC$_{22}$**

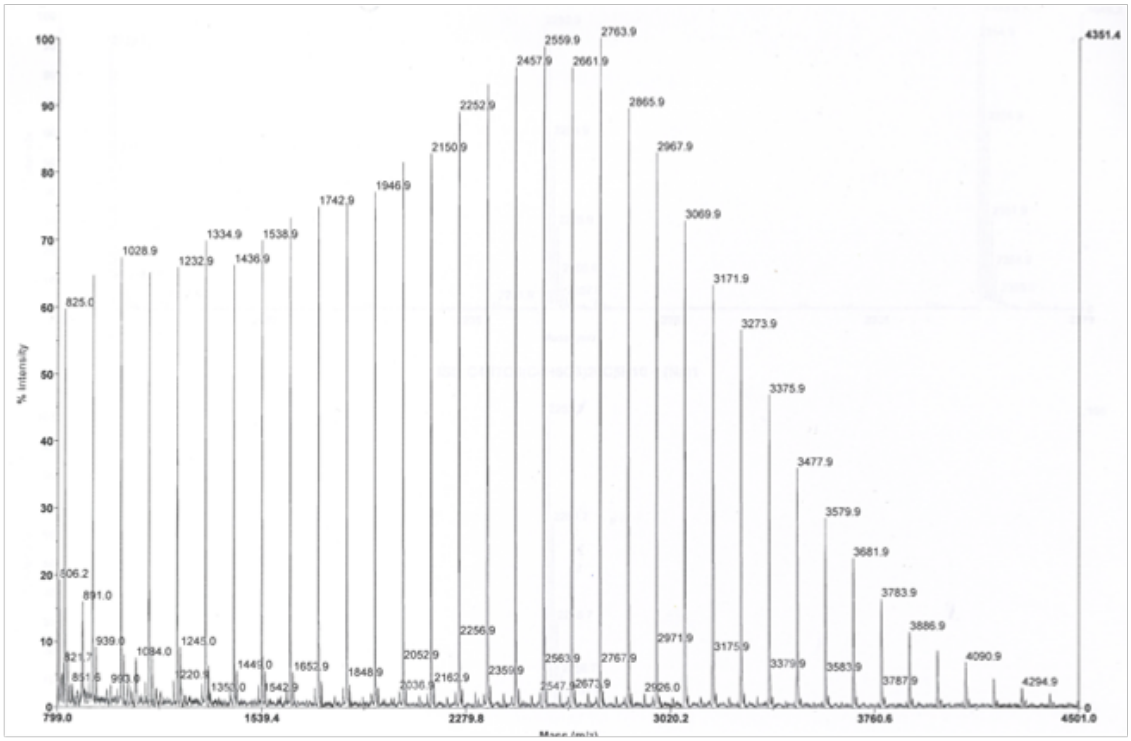

**Figure S7: MALDI-TOF spectrum of Mal-PTMC$_{30}$ (theoretical monocharged peak [M+Na]$^+$ = 3386.07 Da)**

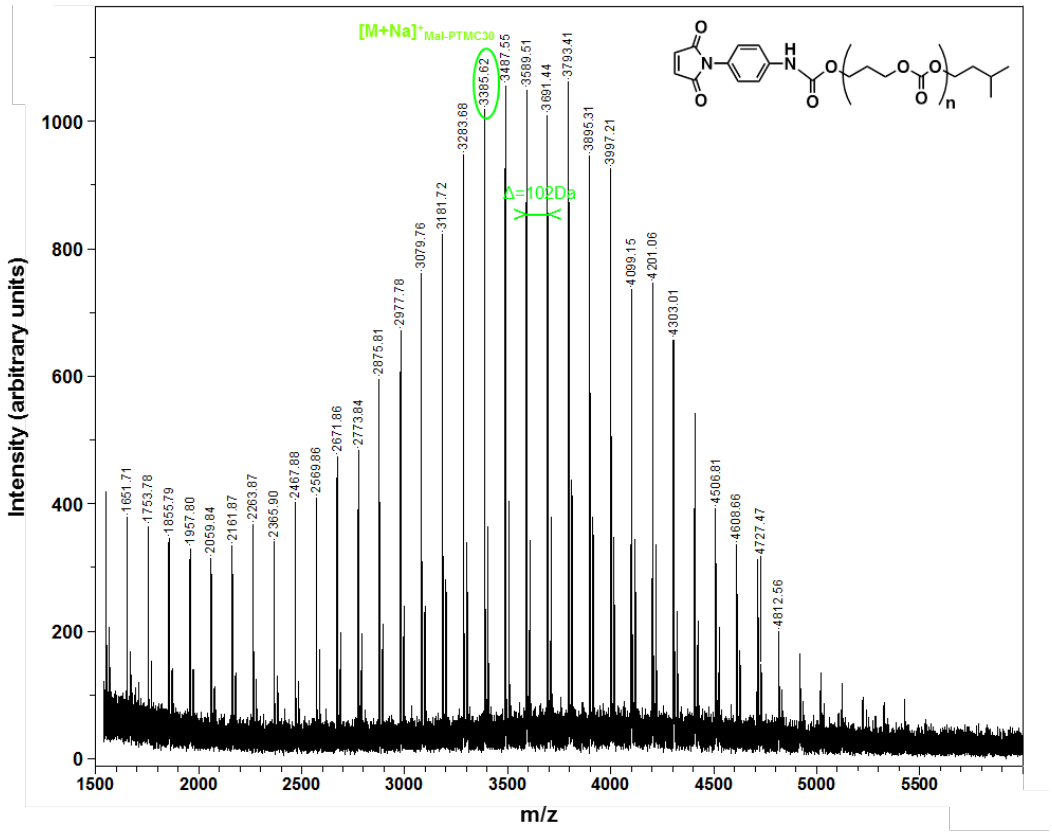


**Figure S8: MALDI-TOF spectrum of Tat peptide (theoretical monocharged peak [M+H]$^+$ = 1733.02 Da)**

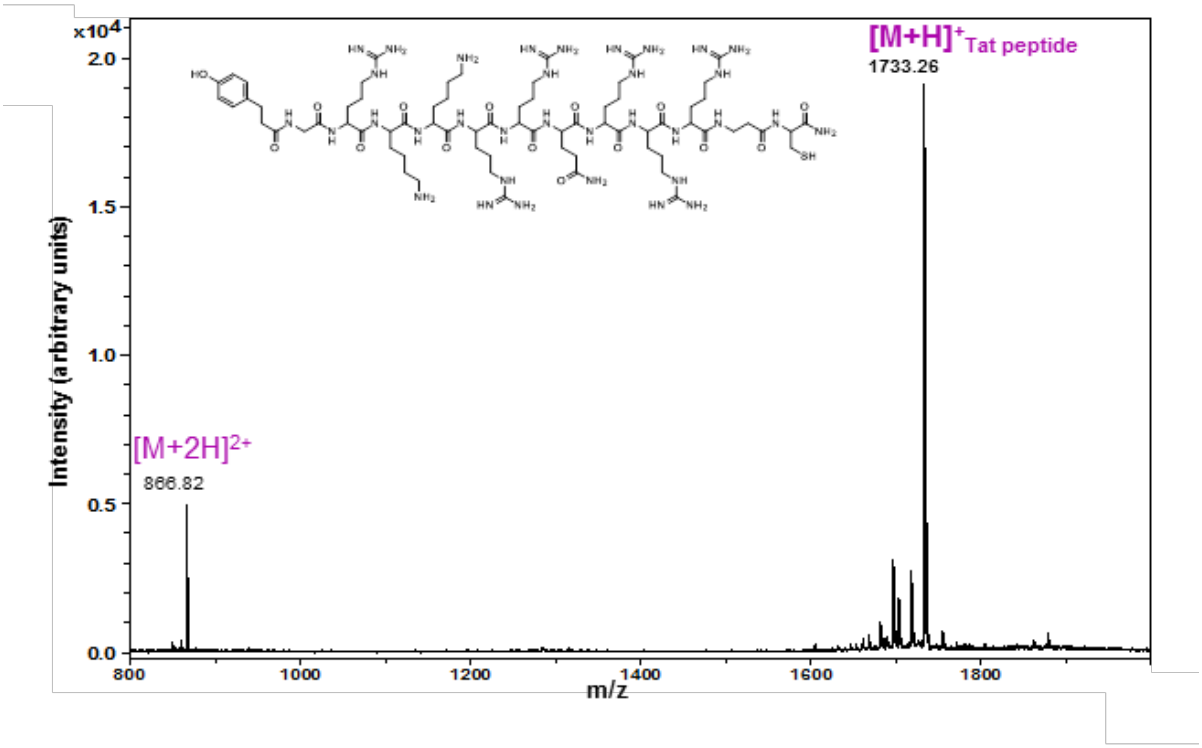

**Figure S9: MALDI-TOF spectrum of Tat-*b*-PTMC$_{30}$ chimera (theoretical monocharged peak [M+H+H$_2$O]$^+$ = 5114.11 Da)**

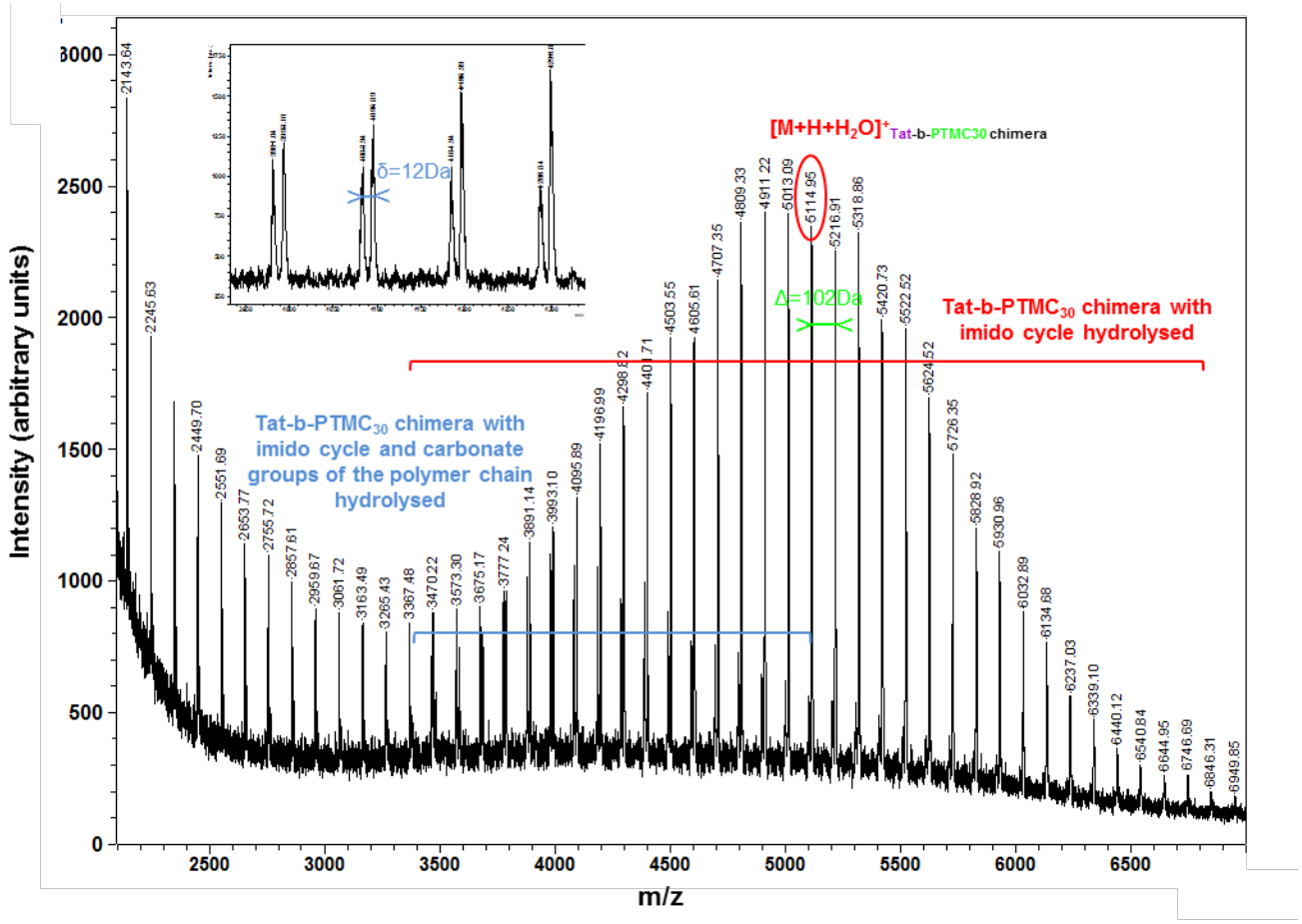


**Figure S10: SEC chromatograms of PTMC homopolymers in THF with RI detection**

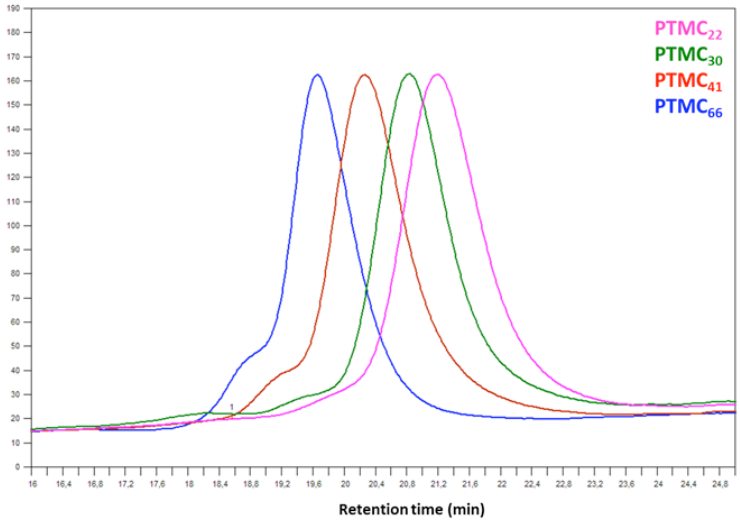


Shoulders observed for higher molar masses are due to coupling of the growing chains occurring at the end of the polymerization. The generated PTMC lacks hydroxyl function so that it can't react afterwards.

**Figure S11: DSC thermograms of $PTMC_{22}$, $PTMC_{30}$, $PTMC_{41}$ (14 months after synthesis) and $PTMC_{66}$ (3 months after synthesis)**

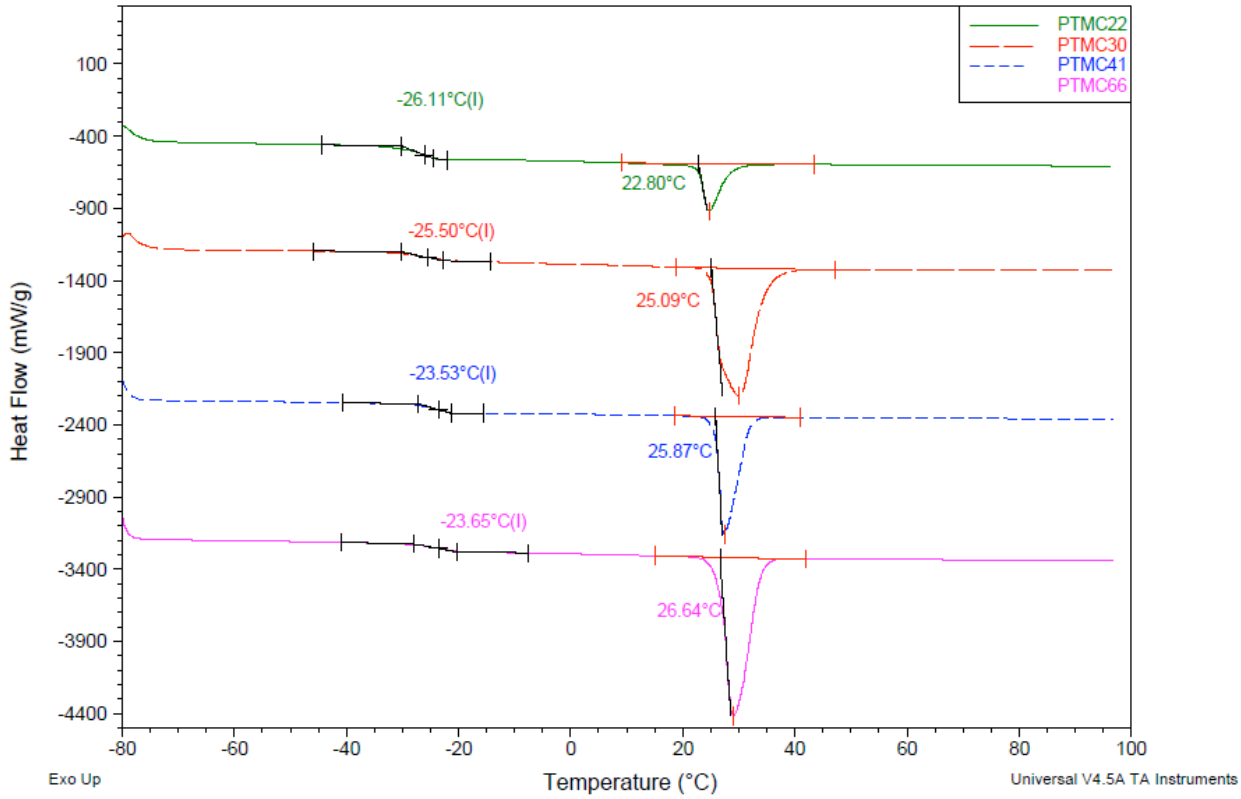


**Figure S12: DSC thermograms of Tat-*b*-PTMC copolymers (2 months after synthesis)**

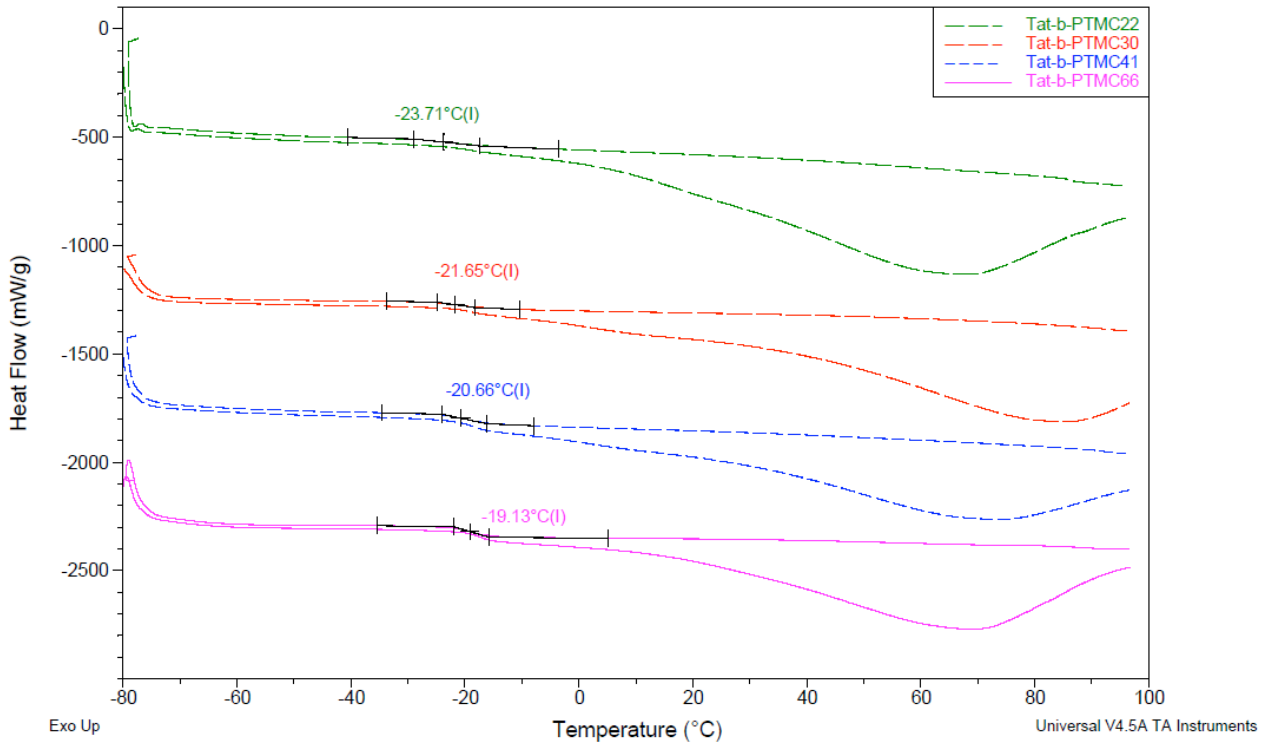

**Figure S13: Atomic Force Microscopy height images and statistical size analysis of Tat-*b*-PTMC nanoparticles. Panel A : Tapping mode AFM images 1x1µm; panel B: Distributions of particles heights; panel C: Distributions of particles diameters**

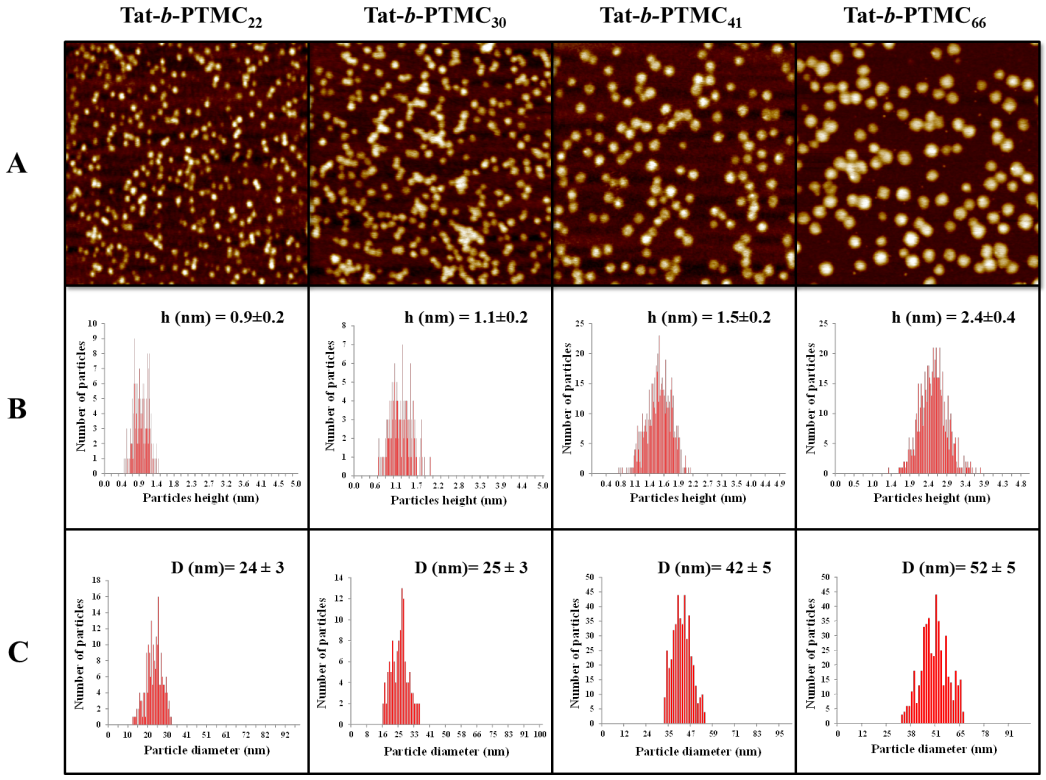


**Table S1: Dimensions from statistical analysis of the disk-like structures observed in AFM (diameter $D_d$ radius $R_d$ and height $h_d$) and estimation of the equivalent micelles radii $R_{AFM}$**

The uniform and distinct spread of particles onto the mica surface allowed a statistical analysis of section dimensions. This spreading can be modelled as a disk-like structure. The radius of micelles ($R_{AFM}$) can then be estimated from the dimensions of the observed disks (diameter D radius R and height h), assuming that the volume of the disks (V) is equal to the volume of spherical micelles ($V_{AFM}$):

Volume of spherical micelle: $V_{AFM} = \frac{4}{3}\pi R_{AFM}^3$

Volume of disk: $V = \pi R^2 h$

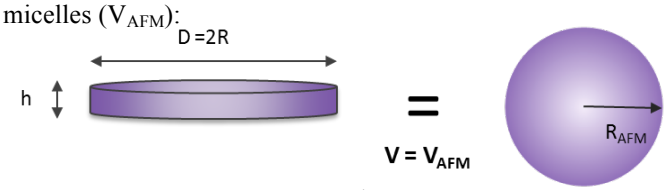


Assuming $V_{AFM} = V$, we obtained: $R_{AFM} = \left(\frac{3}{4}R^2 h\right)^{\frac{1}{3}}$

Standard deviation calculation: $\frac{\Delta R_{AFM}}{R_{AFM}} = \frac{2}{3}\frac{\Delta R}{R} + \frac{1}{3}\frac{\Delta h}{h}$

As hydrodynamic radii ($R_H$, Table 1) were significantly larger than those calculated by AFM (approximately twice), we assumed that the solvation shell of the nanoparticles was rather significant, complying with the cationic nature of the hydrophilic layer.

| DPn | D | R | h | $R_{AFM}$ |
|---|---|---|---|---|
| 22 | 24±3 | 12±2 | 0.9±0.2 | 4.6±0.8 |
| 30 | 25±3 | 12.5±1.5 | 1.1±0.2 | 5.1±0.7 |
| 41 | 42±5 | 21±3 | 1.5±0.2 | 7.9±1.1 |
| 66 | 52±5 | 26±3 | 2.4±0.4 | 10.7±1.4 |

**Experimental Section: Transmission Electron Microscopy**

TEM images were recorded at Bordeaux Imaging Center (BIC) on a FEI TECNAI 12 microscope working at 120 kV equipped with a GATAN Orius 11 MP camera. Samples were prepared by spraying nanoparticle dispersions in ultra-pure water (0.1 $mg.mL^{-1}$) onto formvar/carbon-coated copper grids (200 mesh) using a tailor-made spray device.

**Figure S14: Microscopy images of Tat-b-PTMC30 micelles. Panel A: Tapping mode AFM images 500x500nm; panel B: TEM micrographs scale bar 200 nm.**

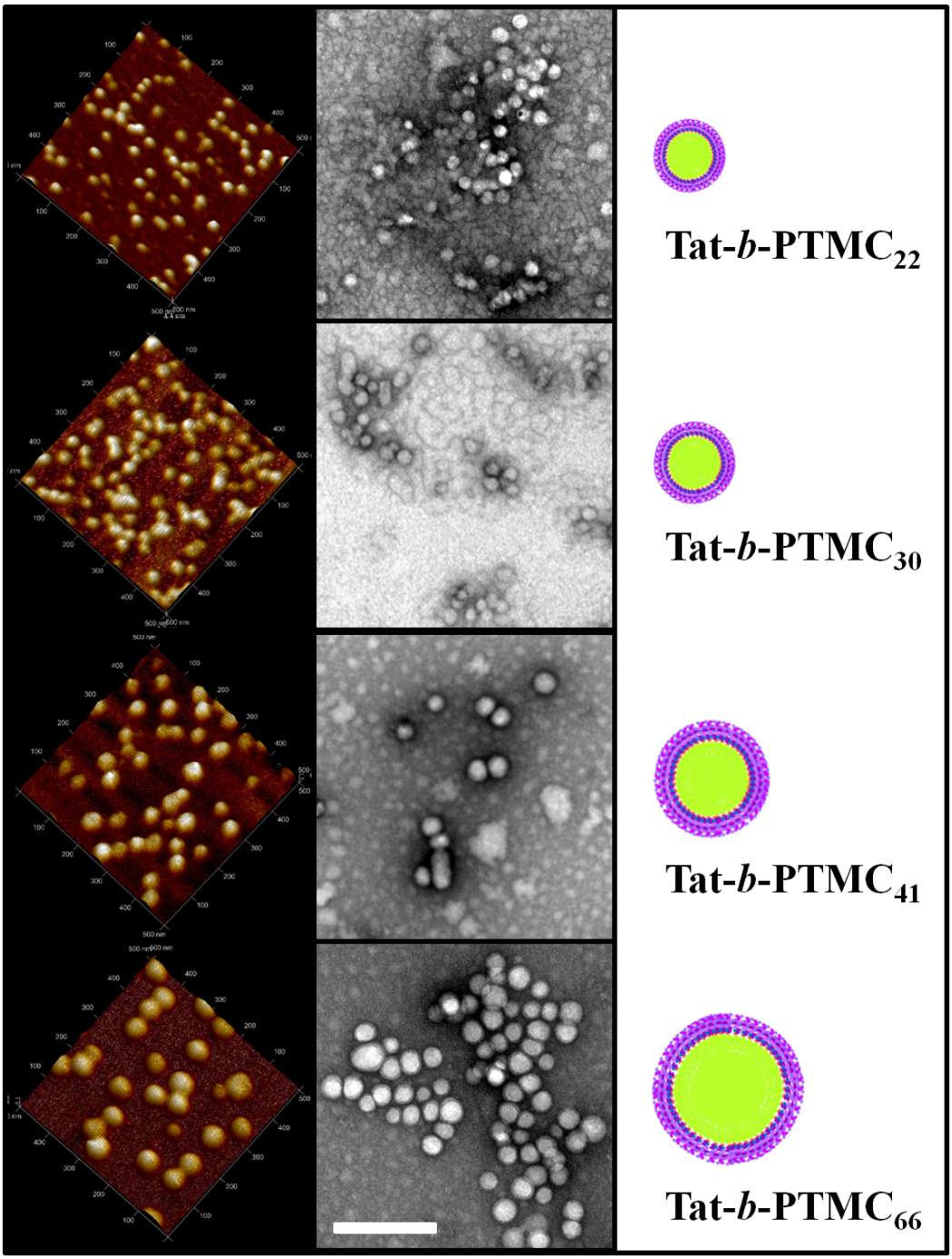

**Figure S15: Multiangle Dynamic Light Scattering analysis of Tat-*b*-PTMC nanoparticles. Panel A: Relaxation curves and corresponding cumulant fits obtained (90°C angle); panel B: Variations of decay rate versus squared scattering vector with linear fits**